Title

Comparative Analysis of Sulfonium−π, Ammonium−π, and Sulfur−π Interactions and Relevance to SAM-Dependent Methyltransferases

Journal

Journal of the American Chemical Society, 144(6)

ISSN

0002-7863

Authors

Albanese, Katherine I
Leaver-Fay, Andrew
Treacy, Joseph W
et al.

Publication Date

2022-02-16

DOI

10.1021/jacs.1c09902

Peer reviewed

HHS Public Access

Author manuscript

J Am Chem Soc. Author manuscript; available in PMC 2023 February 16.

Published in final edited form as:

J Am Chem Soc. 2022 February 16; 144(6): 2535–2545. doi:10.1021/jacs.1c09902.

Comparative Analysis of Sulfonium-π, Ammonium-π, and Sulfur-π, Interactions and Relevance to SAM-dependent Methyltransferases

Katherine I. Albanese[1], **Andrew Leaver-Fay**[2], **Joseph W. Treacy**[3], **Rodney Park**[2], **K. N. Houk**[3], **Brian Kuhlman**[2], **Marcey L. Waters**[1,*]

[1]Department of Chemistry, CB 3290, University of North Carolina at Chapel Hill, Chapel Hill, NC, 27599

[2]Department of Biochemistry and Biophysics, School of Medicine, University of North Carolina at Chapel Hill, Chapel Hill, NC, 27599

[3]Department of Chemistry and Biochemistry, University of California Los Angeles, Los Angeles, CA, 90095-1569

Abstract

We report the measurement and analysis of sulfonium-π. thioether-π and ammonium-π interactions in a β-hairpin peptide model system, coupled with computational investigation and PDB analysis. These studies indicated that the sulfonium-π interaction is the strongest, and that polarizability contributes to the stronger interaction with sulfonium relative to ammonium. Computational studies demonstrate that differences in solvation of the trimethylsulfonium versus the trimethylammonium group also contribute to the stronger sulfonium-π interaction. In comparing sulfonium-π versus sulfur-π interactions in proteins, analysis of SAM- and SAH-bound enzymes in the PDB suggest that aromatic residues are enriched in close proximity to the

*Corresponding Author Marcey L. Waters - Department of Chemistry, CB 3290, University of North Carolina at Chapel Hill, Chapel Hill, North Carolina 27599, United States; mlwaters@email.unc.edu.

Author Contributions

The manuscript was written through contributions of all authors. All authors have given approval to the final version of the manuscript.

ASSOCIATED CONTENT

Supporting Information

The Supporting Information is available free of charge on the ACS Publications website.

Synthesis methods and characterization of materials (LCMS and NMR), computational and bioinformatics methods, coordinates for interaction energy calculations, and additional statistics from PDB analysis. (PDF)

AUTHOR INFORMATION

Katherine I. Albanese - Department of Chemistry, CB 3290, University of North Carolina at Chapel Hill, Chapel Hill, North Carolina 27599, United States; https://orcid.org/0000–0002-2336–1621

Andrew Leaver-Fay - Department of Biochemistry and Biophysics, School of Medicine, University of North Carolina at Chapel Hill, Chapel Hill, NC, 27599

Joseph W. Treacy - Department of Chemistry and Biochemistry, University of California Los Angeles, Los Angeles, CA, 90095–1569

Rodney Park - Department of Biochemistry and Biophysics, School of Medicine, University of North Carolina at Chapel Hill, Chapel Hill, NC, 27599

K. N. Houk - Department of Chemistry and Biochemistry, University of California Los Angeles, Los Angeles, CA, 90095–1569

Brian Kuhlman - Department of Biochemistry and Biophysics, School of Medicine, University of North Carolina at Chapel Hill, Chapel Hill, NC, 27599

Notes

The authors declare no competing financial interest.

sulfur of both SAM and SAH, but the population of aromatic interactions of the two cofactors are not significantly different, with the exception of the Me-π interactions in SAM, which are the most prevalent interaction in SAM but are not possible for SAH. This suggests that the weaker interaction energies due to loss of the cation-π interaction in going from SAM to SAH may contribute to turnover of the cofactor.

Graphical Abstract

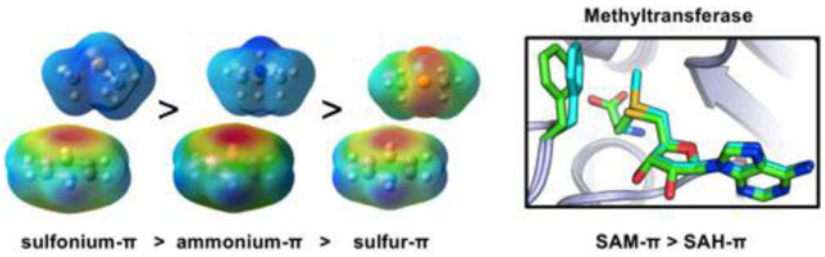

INTRODUCTION

Cation-π interactions, defined as the favorable interaction between a cationic species and the electron-rich face of an aromatic ring or other π system are well established to contribute to biomolecular structure and function.[1–5] Their role in mediating crucial biological processes such as catalysis, protein folding, and protein-ligand and protein-protein interactions has led to extensive characterization of ammonium-based cation-π interactions using statistical analyses of protein structures, gas phase measurements, computational models, and experimentally determined interaction energies with different aromatic residues in a number of protein contexts.[1–7] Sulfonium cations, such as S-adenosylmethionine (SAM) and S-methylmethionine (Mme) (Figure 1), are also important drivers of biomolecular function. Thus, understanding how sulfonium-π interactions compare to both ammonium-π interactions and thioether-π interactions is important for understanding their role in a biological context. Recently, there have been numerous reports on sulfur based aromatic interactions in the context of protein structures, including thioether-π[8–13], thiol-π[12, 14–15], sulfoxide-π[16–17] and sulfone-π[17] interactions. However their cationic counterpart, the sulfonium-π interaction, has been less comprehensively investigated, particularly in comparison to the isosteric ammonium-π interaction.[18–25] Herein, we compare sulfonium-π interactions to both ammonium-π interactions and thioether-π interactions within a β-hairpin model system and through computational studies. Furthermore, we analyze data from the protein data bank (PDB) to gain insight into how the energetic differences of sulfonium-π and sulfur-π interactions influence structure and function of SAM-dependent proteins.

Comparing the central atom in alkylated ammonium and sulfonium cations, sulfur is more polarizable, and the C-S bonds are longer than C-N, such that a trialkylsulfonium has greater surface area and polarizability than a trialkylammonium (Table 1). However, nitrogen is more electronegative than sulfur, therefore there is a greater partial positive charge on the N-methyls relative to nitrogen, while in sulfonium cations, the positive charge is localized on the sulfur (Table 1). In the context of studying these interactions in an aqueous environment,

it is also important to note that trialkylammonium has the potential to form favorable hydrogen bonds in water, which may affect both the desolvation cost to pack against the face of the aromatic ring, as well as the strength of the cation-π interaction itself, whereas a trialkylsulfonium does not form appreciable hydrogen bonds.[26] Each of these subtle differences may influence the magnitude of the cation-π interactions.

Calculations of gas phase and solvated alkali metal cation-π interactions offer insights into trends one may expect of the relative strength differences between alkylated ammonium- and sulfonium-π interactions. For gas phase calculations with alkali metals, it is well established that as the size of the cation increases, the cation-π interaction weakens because the charge becomes more dispersed ($Li^+ > Na^+ > K^+$), exemplary of an electrostatic interaction.[27] However, for calculations performed in a full hydration shell, the heavier alkali metal cation-π interaction strengths are less affected by solvation and the interaction energies are nearly equal for Li^+, Na^+, and K^+.[28–30] Whether the same trend holds true for alkylammonium and alkyl sulfonium ions has not been determined.

Several previous studies have investigated sulfonium-π interactions in binding[20, 23] and catalysis.[18–19, 31–32] However, little work has compared the energetics of sulfonium-π versus ammonium-π interactions, particularly in the same alkylation state.[20, 32] Comparison of two structurally different ligands containing an ammonium or sulfonium moiety binding to a molecular tweezer suggests that the sulfonium compound binds more tightly, but other variations in the two structures may contribute to this difference in binding energy.[20] Only one report directly compares a sulfonium to an ammonium in the same alkylation state, in a comparison of SAM decarboxylase inhibitors, and found that the IC_{50} for the ammonium was 1.5–5-fold more favorable than for the sulfonium, counter to trends predicted from solvated alkali metals.[25]

The studies reported herein provide new mechanistic insights into the magnitude and driving force of the two cationic species. Using a well-established peptide model system, we have investigated the interactions of S-methylmethionine (Mme) and its isostere, 2-amino-4-(dimethylamino) butanoic acid (Dabme2), with Trp, Tyr, and Phe to determine the effect the central atom has on the magnitude and driving force of the cation-π interactions. We also measured the differences in tunability of the interaction with respect to the chemical nature of the aromatic residue. Additionally, we have compared these interactions to Met-π interactions, which have been previously studied in the Waters lab with Trp and Phe[8] but have expanded here to include Tyr as well. Herein, we find that sulfonium-π interactions are more favorable than both alkylammonium-π and Met-π interactions by nearly 1 kcal/mol. Analysis of the driving forces that contribute to both cation-π interactions suggests that the sulfonium-π interaction may have a greater dispersive term than the ammonium-π interaction, consistent with other sulfur-mediated noncovalent interactions.[8–13] Our computational studies suggest that differences in solvation of the ammonium versus sulfonium ion also contribute to the differences in interaction energy. Furthermore, PDB analysis of SAM- and SAH-binding proteins suggests that the difference in magnitude between sulfur-π and sulfonium-π interaction strength influences the mechanism of methyltransferase enzymes that use these cofactors for their biological function. Together, these analyses elucidate the role of the central cationic atom in cation-π

interactions and how proteins may use the difference in energy of thioether-π vs sulfonium-π interactions for turnover.

RESULTS AND DISCUSSION

Investigation in a β-Hairpin Model System.

System Design.—The peptides X2M, X2Mme, and XDabme2 (where X is Trp, Tyr, and Phe at position 2) were used to investigate the role of the central cationic atom on the cation-π interaction with an aromatic amino acid, X (Figure 2). This peptide sequence has been used to investigate a wide range of aromatic interactions, including cation-π and sulfur-π interactions[8], among others, and has proven to be a robust model system for the investigation of noncovalent interactions. β-hairpins serve as good model systems for studying biologically relevant noncovalent interactions because the sidechain-sidechain interactions contribute to folding, and the folding equilibrium can be determined in a straight-forward manner based on NMR chemical shifts. The residues of interest were placed at the 2 and 9 positions to allow for a favorable diagonal sidechain-sidechain interaction.[33–34] The overall charge was +1 to +2 to provide solubility and prevent aggregation, and an Asn-Gly type I' turn was used to promote hairpin formation. Additionally, β-branched amino acids were placed on the opposite face as the residues of interest to stabilize the structure due to their high β-sheet propensity as well as cross-strand hydrophobic interactions that bury the hydrogen bonds and stabilize the structure.[35] This is particularly important in this system, as we have shown in other β-hairpin studies in our lab that shorter, charged sidechains, like Mme and Dabme2, have low β-sheet propensity, so while they may provide stability to the diagonal interaction being investigated, they are destabilizing to the overall hairpin.[36]

X2 and Z9 are positioned diagonally cross-strand on the non-hydrogen bonding face of the β-hairpin, which places them in close proximity due to the right-handed twist of the β-hairpin. Since favorable sidechain-sidechain interactions contribute to hairpin stability, the extent of folding of a peptide is a measure of noncovalent interactions between the two sidechains of interest. Double mutant cycles (Figure 3) were used to isolate the interaction energy between the two sidechains by correcting for other structural effects such as β-sheet propensity, which are particularly low for Mme and Dabme2.[37] The X2 position was substituted with Val and the Z9 position with Ser for the single and double mutants, as has been reported previously, since both have high β-sheet propensities but no favorable interactions (Figure 3).[36]

Characterization of β-Hairpin Structure.—These peptides were synthesized using standard methods and their structures were characterized by NMR, including TOCSY, NOESY, and variable temperature experiments. We validated that the peptides take on the expected β-hairpin conformation based on the parent peptide[8, 36, 38–41], including expected cross-strand and sidechain-sidechain NOEs (Figure S18–20). Additionally, downfield shifting of the Hα protons relative to random coil shifts was determined, as shifting of > 0.1 ppm, demonstrates β-sheet conformation.[42–43]As expected, the residues designed to be in the strands exhibited significant downfield shifting, whereas the turn residues and N-

and C-terminal residues, which are typically frayed, exhibit little change in chemical shift. (Figure S17).

Characterization of β-Hairpin Stability.—To complete the double mutant cycle and determine the sidechain-sidechain interaction energy, the stability of each β-hairpin was determined by NMR using reported methods.[42–45] Based on these values, the Trp peptides are the most folded, with WM found to 88% folded, WMme 64% folded, and WDabme2 57% folded (Table 2). Comparisons with the other aromatic residues at X2 follow similar trends. Fraction folded provides insight into the net stabilities of the peptides, but it is not indicative of the strength of the isolated sidechain-sidechain interaction, since other factors such as β-sheet propensities also influence folding. Short, charged residues, including Dabme2, have previously been shown to have poor β-sheet propensities,[36, 46] so, further analysis of the free energies measured from the double mutant cycle is necessary to characterize the magnitude of the Met-, ammonium-, and sulfonium-π interactions.

Characterization of Magnitude of Diagonal Interactions between X2 and Z9.—The magnitudes of the sidechain-sidechain interactions were determined from the double mutant cycles as described above (Figure 3 and Table S3). The interaction energies are the strongest for Trp, as expected for the larger, more electron-rich ring. The interactions with Mme were strongest for all aromatic rings and the interaction energy was determined to be 1.4 kcal/mol for WMme. The WM interaction energy is weaker than the sulfonium-π interaction by about 1 kcal/mol, and within error of the WDabme2 interaction (Table 3), consistent with previous reports comparing Met S-π (−0.3 ± 0.1 kcal/mol) to Lys cation-π interactions (−0.3 ± 0.1 kcal/mol).[8] The trends are consistent notwithstanding changes in the aromatic residue; the sulfonium-π interaction is still the most favorable, but Met-π, sulfonium-π, and ammonium-π are all weaker when diagonal from Phe and Tyr compared to Trp. There are two important takeaways from these results: sulfonium-π interactions are stronger than ammonium-π interactions when comparing isosteric cations, and sulfonium-π interactions are stronger than thioether-π interactions. Each of these findings were investigated in more detail as described below.

Characterization of Noncovalent Driving Forces Contributing to Sidechain-Sidechain Interactions.—While cation-π interactions are driven by a significant electrostatic component, other forces also contribute to the interactions of cations with aromatic rings. In particular, Dougherty pointed out that for organic cations, such as NMe_4^+, there may be a significant dispersion term associated with the significant polarizability of the cation. To evaluate whether the differences between the sulfonium- and ammonium-π interactions arise from differences in dispersion forces, the interaction energy (ΔΔG°) was plotted against polarizability of the aromatic residue (Figure S21B). Positive correlations are observed for polarizability with both cations (Figure S21B). These results suggest that both cation-π interactions are sensitive to polarizability, which is consistent with previous work indicating a significant dispersive term to cation-π interactions.[3] Since sulfur is more polarizable than nitrogen, this suggests that Mme may have a larger dispersive term than Dabme2.[9, 47–48]

Structural Characterization of the Sidechain-Sidechain Interactions.—The proximity and geometry of these interactions is directly tied to the fraction folded of each respective β-hairpin because the changes in chemical shift are indicative of the population of folded states that has those residues in close proximity to one another. Thus, to confirm that the differences in interaction energy result from specific noncovalent interactions, we compared the anisotropic effects on Met, Mme, and Dabme2 arising from proximity to the face of the Trp to assess the geometry of the sidechain-sidechain interaction. Proximity of a proton to the face of an aromatic ring results in upfield shifting of the proton resonance in the NMR spectrum. Examining the differences in shifting for each Z9 sidechain thus provides insight into the proximity and preferred geometry of interaction with the X2 position. Comparing differences in WZ9 interactions, Mme experiences the most upfield shifting, followed by Dabme2 then Met (Figure 4). The fact that Met exhibits the least upfield shifting is surprising, since it is the most folded peptide and the degree of shifting is not only influenced by the magnitude of the diagonal interaction, but also by the population of the folded state. Thus, the lower degree of upfield shifting for Met strongly supports its weaker interaction with Trp.[8] These findings suggest that the cation in Mme and Dabme2 provides a stronger anchoring point for interaction with the aromatic ring, while Met provides a weaker anchoring point, leading to smaller averaged chemical shift differences.

For Mme and Dabme2, the ε-methyl groups experience the greatest upfield change in chemical shift, 0.4 ppm and 0.3 ppm respectively, consistent with partial positive charge on the methyls (Figure 1) interacting directly with face of Trp (Figure 4). The γ-methylenes, which also carry a partial positive charge, show some upfield shifting as well (Figure 4). These results indicate that the Mme-π interaction is more populated than the Dabme2-π interaction. PDB and computational analyses for cation-π interactions define the most prevalent geometry as the N-methyls of alkylated ammonium cations directed normal to the aromatic ring, and that the strength of the interaction increases with more favorable N-methyl contacts, and the same would be expected for alkyl sulfoniums.[4, 49–50]

Thermal Denaturation Studies.—To further evaluate the nature of the noncovalent interactions for the X2Z9 diagonal interactions, we performed thermal denaturation studies with the WZ9 peptides and fit the changes in fraction folded with respect to temperature to the van't Hoff equation (Figure 5). Compared to WMme and WDabme2, folding for WM is less entropically unfavorable, and exhibits cold denaturation, consistent with a greater hydrophobic driving force (Table 4). Folding of both WMme and WDabme2 is more enthalpically favorable, entropically unfavorable, and does not exhibit cold denaturation (Table 4). This is consistent with the contribution of an enthalpically favorable cation-π interaction for both Mme and Dabme2.[3, 38, 51]

Summary of β-hairpin studies.—In summary, the experimental studies from the β-hairpin model system indicate that both cation-π interactions with sulfonium and ammonium contribute to folding enthalpically whereas the Met-π interaction contributes entropically. Upfield shifting corroborates the preference for an interaction geometry that allows for cation-π interactions with Mme and Dabme2, but not Met. Comparison of the two cation-π interactions indicates that the sulfonium-π interaction is stronger than the

ammonium-π interaction and that greater sensitivity to polarizability contributes to this preference. We then turned to computational methods to gain further insight into additional factors that contribute the difference in sulfonium-π vs ammonium-π interactions.

Computational Analysis of Mme and Dabme2 with Benzene

To gain insight into the role of solvation on the difference in interaction energies between the Mme-π and Dabme2-π interactions, we performed interaction energy (E_{int}) calculations on the optimized conformers for trimethylsulfonium and trimethylammonium with benzene in the presence of N = 0–2 water molecules in implicit solvent (Figure 6). Previous studies of alkali metals found that aqueous solvation changed the relative stabilities of cation-π interactions, with the larger cations becoming more favorable in water.[28–30] The effects of solvation have been previously computed for ammonium and sulfonium ions alone, but not for sulfonium in the presence of a π-system.[52–53] In accordance with similar studies, only the alkylated heteroatom and a benzene ring were implemented for E_{int} calculations.[12, 17, 49]

When N = 0 waters, the preferred geometry for trimethylsulfonium places the sulfur down, 3.2 Å directly over the center of the ring and the S-methyls pointed away, ranging from 4–4.8 Å from the ring (Figure 6B). For trialkylammonium, the NH is 2.1 Å away pointed directly at the center of the ring, and the N-methyls are pointed upward, 3.8 Å away (Figure 6E). In both cases, the lowest energy conformer places the highest concentration of positive charge (Figure 6A) in close contact to benzene. At N = 0, though the S of the alkylated sulfonium ion has a greater positive charge, the sulfonium is a larger, more polarizable cation and with the distances from the benzene ring being farther and the charge more dispersed, the NH-π interaction is stronger than the sulfonium-π interaction. The calculated values of E_{int} favor the ammonium over the sulfonium by 2 kcal/mol, (−6.8 kcal/mol and −4.8 kcal/mol respectively), and these relative differences are comparable to what has been previously reported in the gas phase for trimethylammonium making a stronger cation-π interaction than the sulfonium.[3, 24] However, these geometries and energetic values are not relevant in water, in which the NH is expected to be highly solvated.

To determine the impact of competitive interactions with water, explicit water molecules were added iteratively and the lowest energy conformers and E_{int} were recalculated, as has been similarly done for methylated ammonium and metal cations.[26, 28–30, 50, 52–53] These calculations show the expected changes in geometry for the trimethylammonium that in turn also weaken the cation-π energy, while much smaller changes were seen for the trimethylsulfonium (Figure 6).

For N = 1, when the NH is participating in a hydrogen bond with water, the geometry changes such that the NH moves away and is directed over the edge of the ring and the N-methyls are within 3.3–4.2 Å from the center of benzene (Figure 6F). The distribution of positive charge also changes such that the NH and N-methyls have a slightly less positive partial charge (Figure 6A). The N = 1 lowest energy conformer favors the N-methyl-π interaction over the NH-π, as the NH-O interaction outcompetes the NH-π interaction. Correspondingly, the E_{int} for the cation-π interaction is significantly less favorable than in the absence of explicit solvent (−4.6 kcal/mol, Figure 6F) from the compounding effects of increased distance from the ring and interaction with a more dispersed charge.[26, 50]

The sulfonium (Figure 6C) also moves away from benzene (3.2 to 3.3 Å), but less than the ammonium cation, and the overall geometry remains the same. The addition of one water weakens the sulfonium-π interaction by only 0.1 kcal/mol, such that the difference in interaction energy between the two alkylated cations favors the sulfonium-π by 0.1 kcal/mol.

The addition of a second water further weakens the interaction for trimethylammonium and trimethylsulfonium, but more subtly for the sulfonium species. Again, the overall geometry of the trimethylsulfonium-benzene interaction does not change, and the distance to the ring increases slightly from 3.3 to 3.4 Å (Figure 6D). The E_{int} for the sulfonium-benzene complex in N = 2 waters is −4.5 kcal/mol. The changes in geometry for the alkylammonium are more dramatic upon the addition of a second water molecule (Figure 6G). The NH is pointed away from the ring such that the N-methyls are pointed down towards the face of the ring, but only one makes contacts to the centroid of benzene (Figure 6G) As previously discussed, the number of N-methyl contacts directly influences the strength of an alkylammonium-π interaction.[49] With the loss of the NH-π interaction, plus the increased distance for the single CH-π interaction with the N-methyl, the E_{int} in N = 2 waters for trimethylammonium is −4.0 kcal/mol, 0.5 kcal/mol weaker than its sulfonium counterpart.

In sum, the experimental results from the β-hairpin studies coupled with the computational studies suggest that the increased polarizability as well as differences in solvation result in a stronger cation-π interaction for sulfonium relative to ammonium ions.

PDB analysis of SAH and SAM Bound Structures

To gain insight into how the energetic differences of sulfonium-π and sulfur-π interactions impact the binding and function of SAM and SAH in SAM-dependent enzymes, we carried out an analysis of SAM- and SAH-bound proteins in the PDB. Analysis of preferred geometries and distances of Lys/Arg-aromatic contacts observed in the PDB has been key to understanding the role of cation-π interactions in biomolecular structure and function.[2, 54–56] These propensities have also been well described for Met and Cys,[9–10, 15, 57] but few studies have compared sulfonium-π to thioether-π interactions in SAM- and SAH-bound enzymes.[21–22]

Ab initio Investigation into Trimethylsulfonium-Benzene Interaction Energies.—Before describing the statistical distributions of these interactions in the PDB, we first calculated the changes in E_{int} for varying distances and angles between trimethylsulfonium and a benzene ring (Figure 7A). The most favorable conformation was calculated to be −4 kcal/mol when the sulfonium cation is at 5° and 3–3.5 Å away from the ring. As the angle moves away from normal to the ring (0°), the interaction becomes weaker and the most favorable geometry moves to greater distances, with interaction energies between −0.2–0 kcal/mol beyond 5 Å (Figure 7A). These regions have been previously defined as en-face ($\theta < 30°$), intermediate ($30° \leq \theta < 60°$), and edge ($60° \leq \theta < 90°$) (Figure 7B).[56] These ranges are similar to what has been previously reported for H_2S, Me_2S, and Me_2SO-benzene complexes as well as guanidinium and ammonium-benzene complexes[56], thereby providing

a guide and cutoff for determining what are nonrandom, enriched contacts within the PDB structures described below.

Aromatic Residues are Enriched and Nonrandomly Oriented in SAM/SAH Binding Sites.—To analyze the sulfonium-π and thioether-π interactions in SAM/SAH binding sites, we compiled a non-redundant set of structures that were bound to either SAM or SAH from the PDB (Table S15). Distances and angles were measured from the Me of SAM, and S, C5', and CG of SAM and SAH to the centroid of nearby aromatic residues, as each of these positions carries a δ+ charge (see Figure 1 for structures and partial charges). We analyzed aromatic residues whose ring centers were within 15 Å of the atoms listed above to maintain consistency with previous analyses on S-π interactions in the PDB.[9, 15] The number of aromatic residues for each atom contact are listed in Table S16. All unique sequences have at least 2 aromatic residues within 15 Å to the aforementioned specified atoms of either cofactor (Figure S26A and B), in agreement with previous reports on the frequency of S-π interactions per structure in the PDB.[9] Additionally, comparison of the aromatic residues His, Tyr, Trp, and Phe indicate that none is preferred in SAH versus SAM binding sites in the investigated structures (Figure S26C).[58]

To evaluate whether aromatic contacts are enriched within SAH/SAM binding sites, we measured how frequently atoms from SAH/SAM make contact (< 4 Å) with an atom from an aromatic residue. The measured values are expressed as percentages, where the value for each atom indicates the percentage of that position that contacts at least one aromatic residue. We compared the sulfur atoms of SAH and SAM and the methyl carbon of SAM against nonpolar amino-acid atoms that are in similar steric environments to our ligands but that are not expected to form specific interactions with an aromatic residue (Figure 8A). The sulfur atom of SAM was compared to the CG atom of Leu. The sulfur atom of SAH was compared to the sulfur of Met and to the CG1 atom of Ile (Figure 8A). We find that SAM S is enriched in aromatic contacts relative to Leu CG, supporting the fact that it forms a specific, favorable interaction (Figure 8B). The S atom of SAH is enriched in aromatic contacts relative to both Ile CG1 and the sulfur of Met in more buried environments (>24 neighbors, Figure 8B, Figure S27), also in agreement that the S of SAH forms specific S-π interactions. Indeed, SAH exhibits differences relative to Met though both contain thioethers that are expected to form equally favorable thioether-π interactions. Such a difference is consistent with SAH-binding proteins having evolved to bind SAM and continuing to hold aromatics in place for that purpose even in SAM's absence.

We compared the methyl group of SAM to the two methyl groups of Leu, which are in a similar steric environment but provide neutral controls (Figure 8A). In this case, no statistically significant difference was observed (Figure 8B). These findings suggest that aromatic interactions with the sulfur atom of SAM are more favorable than interactions with the methyl group, which is consistent with our computational results described above.

After confirming that there is an enrichment of aromatic residues in the neighborhoods surrounding the sulfonium and thioether of SAM and SAH, we examined the angular preferences for aromatic contacts by measuring *contact densities*, the average number of aromatic-ring centers per $Å^3$, for each of the Me, S, C5', and CG groups. We divided

conformation space into the three angle bins described above (en-face, intermediate, & edge) and into three distance bins: 3–5, 5–8, and 8–15 Å and further divided each of these 9 bins with a distance step size of 0.5 Å and an angular step size of 5° (Figures S28–S34). This fine binning better emphasizes geometrically improbable conformations, such as those at very close distances or at angles very near 0°, where the volumes of the bins are very small. *Average contact density* for a large bin was computed as the average of the contact densities of each of the small bins it contained. The large bins facilitate comparison with previous PDB and computational analyses characterizing S-π interactions.[12, 15, 17]. The percentage of observed average contact densities in the PDB (Figure 9A) in the 3–5 Å range (Figure 10A) indicate a preference for en-face and intermediate geometries at each of the positions of SAM and SAH, with some variation depending on position. Edge interactions (angles > 60°) (Figure 9A, Figures S28–S34) are the least common orientation for all for positions in SAM or SAH, as expected for contacts driven by cation-π and sulfur-π interactions, which require an en-face or intermediate geometry.[3, 15] In particular, Figure S35, which evaluates the entire 15 Å range, shows that the average contact density is significantly higher for distances below 5 Å where sulfonium-π and thioether-π interactions are favorable, and that smaller angles are also preferred.

While this is suggestive of more favorable interactions at smaller angles, we wanted to evaluate whether sterics could also explain the low probability of edge interactions, given that the minimum collision-free distance increases as the angle increases. To evaluate the contribution of sterics to the contact density of en-face, intermediate, and edge interactions, we sampled random orientations between the four aromatic amino acids and each ligand, SAM and SAH, and measured the distances and angles, excluding conformations that contained clashes (Figure 9B).

When compared, the observed preferences for en-face and intermediate geometries in the PDB (Figure 9A, Figure S35) are greater than predicted for random interactions (Figure 9B) and are consistent with the idea these interactions are not random, but prefer specific geometries. Furthermore, the observed preference for en-face interactions agree well with the most favorable geometries predicted by our *ab initio* studies (Figure 8). The random average contact densities were found to be between a six- and eight-fold greater (depending on the atom) for en-face over edge geometries at distances < 5 Å for each atom (Figure 9B), which is smaller than the 6- to 26-fold increases (depending on the atom) of en-face over edge geometries observed in the PDB (Figure 9A, Table S17), indicating that sterics alone cannot explain the angular preferences. In particular, SAM Me and C5’ show the strongest preference for en-face over edge geometries. Additionally, comparison of S, C5’, and CG in both SAM and SAH indicate that these atoms make more en-facecontacts to SAM in all cases (Figure 9A, white bars). Figure 10 displays representative geometries for each of these interactions.

In comparing SAM to SAH, we wanted to account for the difference in number of atoms surrounding sulfur. Therefore, we computed the *average contact density per atom* (the sum of average contact densities for each atom in the cofactor divided by the number of cofactor atoms) for all fine bins within 3–5 Å for SAM and SAH. We find that even when accounting for the number of atoms, average contact density per atom is 21% higher

for SAM than for SAH (Table S17). We considered that the Me group is more sterically accessible than the other three groups in SAM, so perhaps its steric accessibility is the source of this greater density. We again employed the random-orientation, collision-free model to answer this question. With this model, which only evaluates steric clashes, the SAM average-contact-density per atom was 27% lower than to SAH, indicating that steric clashes disfavor aromatic interactions with SAM relative to SAH. This suggests that the *21% greater* interactions to SAM versus SAH reflects a greater energetic preference for favorable aromatic interactions to SAM.

Taken together, the greater en-face aromatic contacts to SAM vs SAH overall and the prevalence of Me-π interactions at en-face geometries (Figures 9A and S35, Table S17), may reflect the role of sulfonium-π vs sulfur-π interactions in enzymatic turnover of SAM-dependent enzymes. For SAM-dependent enzymes to function catalytically, they need to unload SAH and reload SAM to transfer another methyl group to the next substrate.[59–61] To do so, the cofactor binding site must have a weaker affinity for SAH relative to SAM. The difference in magnitude between the sulfonium-π and S-π interactions of SAM and SAH, as well as the difference in contact density of aromatic interactions between the two cofactors, may contribute to the driving force for product release. From our β-hairpin results, we calculated the WMme sidechain-sidechain interaction to be ~ 1 kcal/mol more favorable than that of WM. Our PDB analyses demonstrate that direct contacts to the Me of SAM make up the greatest percentage of interactions to the cofactor within 3–5 Å, thus, upon transfer of the methyl group of SAM, SAH will have both fewer and weaker interactions, thus weakening binding and promoting turnover of the cofactor. Figure 11 displays an overlay of SAM and SAH in the same protein, demonstrating such a loss of aromatic interaction with SAH.

CONCLUSIONS

Herein we utilize a peptide model system, computational studies, and analysis of the protein data bank to evaluate the chemical and biological relevance of sulfonium-π interactions as compared to ammonium-π and sulfur-π interactions. Experimental determination of interaction energies in aqueous solution indicates that sulfonium-π interactions are stronger than the isosteric ammonium-π interactions as well as the neutral sulfur-π interactions. Computational studies indicate that differences in solvation of the ammonium and sulfonium groups contribute to the differences in magnitude of interaction. Analysis of the protein data bank provides insight into how the difference in sulfonium-π and sulfur-π interaction energies contribute to biological function in SAM-dependent methyltransferases. We find that SAM and SAH are enriched for aromatic contacts relative to control residues that interact nonspecifically, and that the preferred geometries are consistent with those expected for energetically favorable cation-π and sulfur-π interactions, respectively. The prevalence and geometries of aromatic interactions at S, CG, and C5’ are similar between SAM and SAH, with the exception the Me-π interaction in SAM, which is the most prevalent of all the interactions, and is not possible with SAH. These findings suggest that sulfonium-π interactions are an important driver in SAM recognition and that weakening and/or loss of sulfonium-π interactions when SAM is converted to SAH weakens binding and aids in the turnover of the cofactor in SAM-dependent methyltransferase enzymes. In sum, the well

correlated results between our β-hairpin model system, computational analysis, and PDB investigation provide both general trends with respect to the magnitude and driving force of ammonium-π, sulfonium-π and sulfur-π interactions, while also providing specific insights into the mechanism by which differences between sulfur-π and sulfonium-π interactions influence enzymatic activity of SAM-dependent methyltransferases.

Supplementary Material

Refer to Web version on PubMed Central for supplementary material.

ACKNOWLEDGMENT

This work was supported by the National Institutes of Health, National Institute of General Medical Sciences R01GM118499 to MLW, R01 GM124480 to KNH, and R35GM131923 to BK. KIA was supported in part by a Burroughs Wellcome Fellowship. This work used computational and storage services associated with the Hoffman2 Shared Cluster provided by UCLA Institute for Digital Research and Education's Research Technology Group.

REFERENCES

1. Kearney PC; Zhang H; Zhong W; Dougherty DA; Lester HA, Determinants of Nicotinic Receptor Gating in Natural and Unnatural Side Chain Structures at the M2 9 Position. Neuron 1996, 17, 1221–1229. [PubMed: 8982168]
2. Dougherty D. a., Cation-pi Interactions in Chemistry and Biology: A New View of Benzene, Phe, Tyr, and Trp. Science 1996, 271, 163–168. [PubMed: 8539615]
3. Ma JC; Dougherty DA, The Cation-π Interaction. Chem. Rev 1997, 97, 1303–1324. [PubMed: 11851453]
4. Gallivan JP; Dougherty DA, Cation-pi interactions in structural biology. Proc. Natl. Acad. Sci 1999, 96, 9459–9464. [PubMed: 10449714]
5. Dougherty DA, The Cation−π Interaction. Acc. Chem. Res 2013, 46, 885–893. [PubMed: 23214924]
6. Baril SA; Koenig AL; Krone MW; Albanese KI; He CQ; Lee GY; Houk KN; Waters ML; Brustad EM, Investigation of Trimethyllysine Binding by the HP1 Chromodomain via Unnatural Amino Acid Mutagenesis. J. Am. Chem. Soc 2017, 139, 17253–17256. [PubMed: 29111699]
7. Krone MW; Albanese KI; Leighton GO; He CQ; Lee GY; Garcia-Borràs M; Guseman AJ; Williams DC; Houk KN; Brustad EM; Waters ML, Thermodynamic consequences of Tyr to Trp mutations in the cation–π-mediated binding of trimethyllysine by the HP1 chromodomain. Chem. Sci 2020, 11 (13), 3495–3500. [PubMed: 34109021]
8. Tatko CD; Waters ML, Investigation of the nature of the methionine-π interaction in β-hairpin peptide model systems. Protein Sci. 2004, 13, 2515–2522. [PubMed: 15322289]
9. Valley CC; Cembran A; Perlmutter JD; Lewis AK; Labello NP; Gao J; Sachs JN, The methionine-aromatic motif plays a unique role in stabilizing protein structure. J. Biol. Chem 2012, 287, 34979–91. [PubMed: 22859300]
10. Reid KSC; Lindley PF; Thornton JM, Sulphur-aromatic interactions in proteins. FEBS Lett. 1985, 190, 209–213.
11. Aledo JC; Cantón FR; Veredas FJ, Sulphur Atoms from Methionines Interacting with Aromatic Residues Are Less Prone to Oxidation. Sci. Rep 2015, 5 (16955), 1–14.
12. Orabi EA; English AM, Modeling Protein S−Aromatic Motifs Reveals Their Structural and Redox Flexibility. J. Phys. Chem. B 2018, 122 (14), 3760–3770. [PubMed: 29533644]
13. Koebel MR; Cooper A; Schmadeke G; Jeon S; Narayan M; Sirimulla S, S···O and S···N Sulfur Bonding Interactions in Protein–Ligand Complexes: Empirical Considerations and Scoring Function. J. Chem. Inf. Model 2016, 56 (12), 2298–2309. [PubMed: 27936771]

14. Forbes CR; Sinha SK; Ganguly HK; Bai S; Yap GPA; Patel S; Zondlo NJ, Insights into thiol-aromatic interactions: A stereoelectronic basis for S-H/π interactions. J. Am. Chem. Soc 2017, 139, 1842–1855. [PubMed: 28080040]
15. Ringer AL; Senenko A; Sherrill CD, Models of S/π interactions in protein structures: Comparison of the H2S-benzene complex with PDB data. Protein Sci. 2007, 16, 2216–2223. [PubMed: 17766371]
16. Lewis AK; Dunleavy KM; Senkow TL; Her C; Horn BT; Jersett MA; Mahling R; McCarthy MR; Perell GT; Valley CC; Karim CB; Gao J; Pomerantz WCK; Thomas DD; Cembran A; Hinderliter A; Sachs JN, Oxidation increases the strength of the methionine-aromatic interaction. Nat. Chem. Biol 2016, 12, 860–866. [PubMed: 27547920]
17. Orabi EA; English AM, Predicting structural and energetic changes in Met–aromatic motifs on methionine oxidation to the sulfoxide and sulfone. Phys. Chem 2018, 20 (35), 23132–23141.
18. McCurdy A; Jimenez L; Stauffer DA; Dougherty DA, Biomimetic Catalysis of SN2 Reactions through Cation-π Interactions. The Role of Polarizability in Catalysis. J. Am. Chem. Soc 1992, 114, 10314–10321.
19. Ngola SM; Dougherty DA, Evidence for the Importance of Polarizability in Biomimetic Catalysis Involving Cyclophane Receptors. J. Org. Chem 1996, 61 (13), 4355–4360. [PubMed: 11667337]
20. Schrader T; Fokkens M; Klärner F-G; Polkowska J; Bastkowski F, Inclusion of Thiamine Diphosphate and S-Adenosylmethionine at Their Chemically Active Sites. J. Org. Chem 2005, 70 (25), 10227–10237. [PubMed: 16323831]
21. Markham GD; Norrby P-O; Bock CW, S-Adenosylmethionine Conformations in Solution and in Protein Complexes: Conformational Influences of the Sulfonium Group. Biochemistry 2002, 41 (24), 7636–7646. [PubMed: 12056895]
22. Bale S; Brooks W; Hanes JW; Mahesan AM; Guida WC; Ealick SE, Role of the sulfonium center in determining the ligand specificity of human s-adenosylmethionine decarboxylase. Biochemistry 2009, 48 (27), 6423–30. [PubMed: 19527050]
23. Ting AY; Shin I; Lucero C; Schultz PG, Energetic Analysis of an Engineered Cation−π Interaction in Staphylococcal Nuclease. J. Am. Chem. Soc 1998, 120 (28), 7135–7136.
24. Hussain MA; Mahadevi AS; Sastry GN, Estimating the binding ability of onium ions with CO2 and π systems: a computational investigation. Phys. Chem 2015, 17 (3), 1763–1775.
25. McCloskey DE; Bale S; Secrist JA; Tiwari A; Moss TH; Valiyaveettil J; Brooks WH; Guida WC; Pegg AE; Ealick SE, New Insights into the Design of Inhibitors of Human S-Adenosylmethionine Decarboxylase: Studies of Adenine C8 Substitution in Structural Analogues of S-Adenosylmethionine. J. Med. Chem 2009, 52 (5), 1388–1407. [PubMed: 19209891]
26. Xu Y; Shen J; Zhu W; Luo X; Chen K; Jiang H, Influence of the Water Molecule on Cation−π Interaction: Ab Initio Second Order Møller−Plesset Perturbation Theory (MP2) Calculations. J. Phys. Chem. B 2005, 109 (12), 5945–5949. [PubMed: 16851648]
27. Dougherty DA, The cation-π interaction. Acc. Chem. Res 2013, 46, 885–893. [PubMed: 23214924]
28. Shakourian-Fard M; Nasiri M; Fattahi A; Vafaeezadeh M, Influence of the water molecules (n = 1–6) on the interaction between Li+, Na+, K+ cations and indole molecule as tryptophan amino acid residue. Struct. Chem 2012, 23 (3), 857–865.
29. Rao JS; Zipse H; Sastry GN, Explicit Solvent Effect on Cation−π Interactions: A First Principle Investigation. J. Phys. Chem. B 2009, 113 (20), 7225–7236. [PubMed: 19402616]
30. Reddy AS; Zipse H; Sastry GN, Cation−π Interactions of Bare and Coordinatively Saturated Metal Ions: Contrasting Structural and Energetic Characteristics. J. Phys. Chem. B 2007, 111 (39), 11546–11553. [PubMed: 17850069]
31. Lin S; Jacobsen EN, Thiourea-catalysed ring opening of episulfonium ions with indole derivatives by means of stabilizing non-covalent interactions. Nat. Chem 2012, 4 (10), 817–824. [PubMed: 23000995]
32. He CQ; Lam CC; Yu P; Song Z; Chen M; Lam Y.-h.; Chen S; Houk KN, Catalytic Effects of Ammonium and Sulfonium Salts and External Electric Fields on Aza-Diels–Alder Reactions. J. Org. Chem 2020, 85 (4), 2618–2625. [PubMed: 31891501]

33. Tatko CD; Waters ML, The geometry and efficacy of cation-pi interactions in a diagonal position of a designed beta-hairpin. Protein Sci. 2003, 12 (11), 2443–52. [PubMed: 14573858]
34. Syud FA; Stanger HE; Gellman SH, Interstrand Side Chain-Side Chain Interactions in a Designed-Hairpin: Significance of Both Lateral and Diagonal Pairings. J. Am. Chem. Soc 2001, 123 (36), 8667. [PubMed: 11535071]
35. Russell SJ; Blandl T; Skelton NJ; Cochran AG, Stability of cyclic beta-hairpins: asymmetric contributions from side chains of a hydrogen-bonded cross-strand residue pair. J. Am. Chem. Soc 2003, 125 (2), 388–95. [PubMed: 12517150]
36. Hughes RM; Benshoff ML; Waters ML, Effects of chain length and N-methylation on a cation-π interaction in a B-hairpin peptide. Chem. Eur. J 2007, 13 (20), 5753–5764. [PubMed: 17431866]
37. Serrano L; Bycroft M; Fersht AR, Aromatic-aromatic interactions and protein stability. Investigation by double-mutant cycles. J. Mol. Biol 1991, 218 (2), 465–75. [PubMed: 2010920]
38. Tatko CD; Waters ML, The geometry and efficacy of cation–π interactions in a diagonal position of a designed β-hairpin. Protein Sci. 2003, 12 (11), 2443–52. [PubMed: 14573858]
39. Tatko CD; Waters ML, Comparison of C-H…π and Hydrophobic Interactions in a-Hairpin Peptide: Impact on Stability and Specificity. J. Am. Chem. Soc 2004, 126 (7), 2028–2034. [PubMed: 14971936]
40. Hughes RM; Waters ML, Influence of N-methylation on a cation-pi interaction produces a remarkably stable beta-hairpin peptide. J. Am. Chem. Soc 2005, 127 (18), 6518–9. [PubMed: 15869257]
41. Hughes RM; Waters ML, Arginine methylation in a beta-hairpin peptide: implications for Arg-pi interactions, DeltaCp(o), and the cold denatured state. J. Am. Chem. Soc 2006, 128 (39), 12735–42. [PubMed: 17002367]
42. Syud FA; Espinosa JF; Gellman SH, NMR-Based Quantification of β-Sheet Populations in Aqueous Solution through Use of Reference Peptides for the Folded and Unfolded States. J. Am. Chem. Soc 1999, 121 (49), 11577–11578.
43. Stanger HE; Syud FA; Espinosa JF; Giriat I; Muir T; Gellman SH, Length-dependent stability and strand length limits in antiparallel β-sheet secondary structure. Proc. Natl. Acad. Sci 2001, 98 (21), 12015. [PubMed: 11593011]
44. Wishart DS; Sykes BD; Richards FM, Relationship between nuclear magnetic resonance chemical shift and protein secondary structure. J. Mol. Biol 1991, 222 (2), 311–33. [PubMed: 1960729]
45. Wishart DS; Sykes BD; Richards FM, The chemical shift index: a fast and simple method for the assignment of protein secondary structure through NMR spectroscopy. Biochemistry 1992, 31 (6), 1647–51. [PubMed: 1737021]
46. Street AG; Mayo SL, Intrinsic β-sheet propensities result from van der Waals interactions between side chains and the local backbone. Proc. Natl. Acad. Sci 1999, 96 (16), 9074–9076. [PubMed: 10430897]
47. Hwang J; Li P; Smith MD; Warden CE; Sirianni DA; Vik EC; Maier JM; Yehl CJ; David Sherrill C; Shimizu KD, Tipping the Balance between S-π and O-π Interactions. J. Am. Chem. Soc 2018, 20, 27.
48. N-M Daeffler K; Lester HA; Dougherty DA, Functionally Important Aromatic−Aromatic and Sulfur−π Interactions in the D2 Dopamine Receptor. J. Am. Chem. Soc 2012, 134, 14890–14896. [PubMed: 22897614]
49. Davis MR; Dougherty DA, Cation–π interactions: computational analyses of the aromatic box motif and the fluorination strategy for experimental evaluation. Phys. Chem. Chem. Phys 2015, 17, 29262–29270. [PubMed: 26467787]
50. Orabi EA; Lamoureux G, Cation−π Interactions between Quaternary Ammonium Ions and Amino Acid Aromatic Groups in Aqueous Solution. J. Phys. Chem. B 2018, 122 (8), 2251–2260. [PubMed: 29397727]
51. Hughes RM; Waters ML, Influence of N-Methylation on a Cation-π Interaction Produces a Remarkably Stable-Hairpin Peptide. J. Am. Chem. Soc 2005, 127, 18. [PubMed: 15631427]
52. Markham GD; Bock CW, Structural and thermodynamic properties of sulfonium ions: an ab initio molecular orbital study. J. Phys. Chem 1993, 97 (21), 5562–5569.

53. Markham GD; Bock CW, The interaction of water with sulfonium ions and the effects of hydration on the energetics of methyl group transfer: An ab initio molecular orbital study of the hydration of (CH3)3S+ and (CH3)2S+CH2CO2−. Struct. Chem 1996, 7 (4), 281–300.

54. Crowley PB; Golovin A, Cation–π interactions in protein–protein interfaces. Proteins 2005, 59 (2), 231–239. [PubMed: 15726638]

55. Li J; Moumbock AFA; Günther S, Exploring Cocrystallized Aromatic Cage Binders to Target Histone Methylation Reader Proteins. J. Chem. Inf. Model 2020, 60 (10), 5225–5233. [PubMed: 32786701]

56. Kumar K; Woo SM; Siu T; Cortopassi WA; Duarte F; Paton RS, Cation–π interactions in protein–ligand binding: theory and data-mining reveal different roles for lysine and arginine. Chem. Sci 2018, 9 (10), 2655–2665. [PubMed: 29719674]

57. Weber DS; Warren JJ, A survey of methionine-aromatic interaction geometries in the oxidoreductase class of enzymes: What could Met-aromatic interactions be doing near metal sites? J. Inorg. Biochem 2018, 186, 34–41. [PubMed: 29807245]

58. Qian W; Yang J-R; Pearson NM; Maclean C; Zhang J, Balanced codon usage optimizes eukaryotic translational efficiency. PLoS Genet. 2012, 8 (3), e1002603-e1002603.

59. Martin JL; McMillan FM, SAM (dependent) I AM: the S-adenosylmethionine-dependent methyltransferase fold. Curr. Opin. Struct. Biol 2002, 12 (6), 783–793. [PubMed: 12504684]

60. Dillon SC; Zhang X; Trievel RC; Cheng X, The SET-domain protein superfamily: Protein lysine methyltransferases. Genome Biol. 2005, 6 (227), 1–10.

61. Kozbial PZ; Mushegian AR, Natural history of S-adenosylmethionine-binding proteins. BMC Struct. Biol 2005, 5 (1), 19. [PubMed: 16225687]

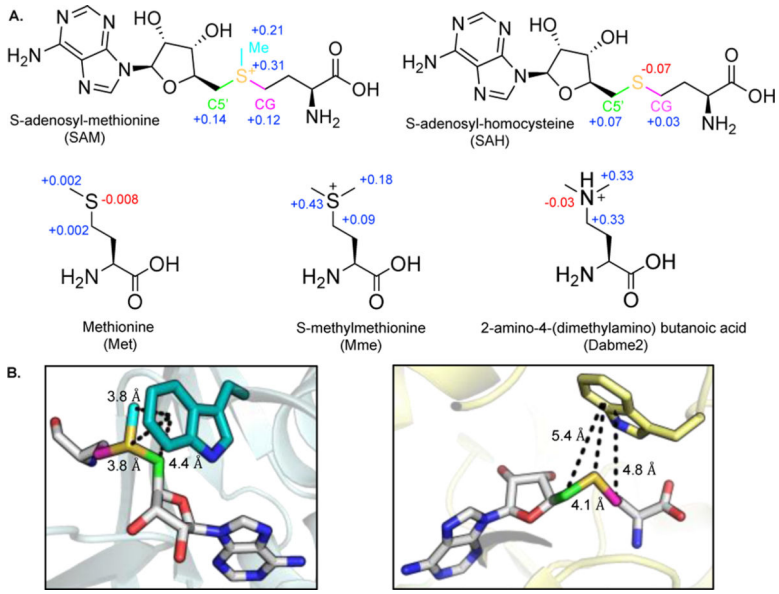

Figure 1.

(A) Structures of S-adenosyl-methionine (SAM), S-adenosyl-homocysteine (SAH), Met, Mme, and Dabme2. Sum of Charge Model 5 (CM5) charges of SAM and SAH were calculated at the M06–2X/6–311+G(d,p) level of theory from coordinates extracted from PDB ID: 3DCM and 3G5T. CM5 partial charges of Met, Mme, Dabme2 calculated at the M06–2X/6–311+G(d,p) level of theory. (B) Trp-SAM interaction (PDB ID: 3MTE) and Trp-SAH interaction (PDB ID: 4NEC).

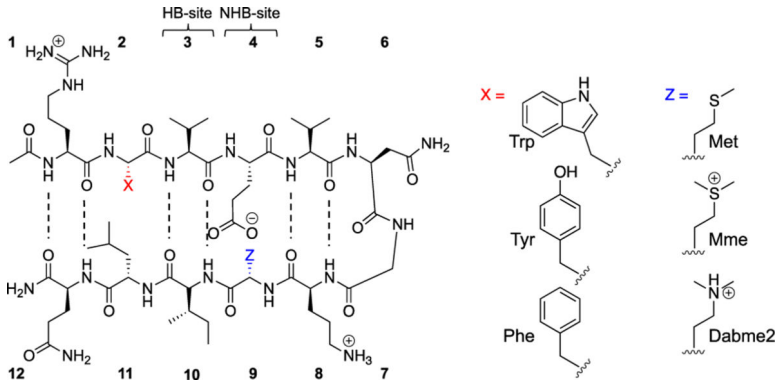

Figure 2.

The 12-amino acid model system (Ac-RX2VEVNGOZ9ILQ-NH_2), where O is ornithine. The diagonal interaction residues are highlighted in red and blue. Peptides are referred to by the diagonal residues X2Z9 in the text.

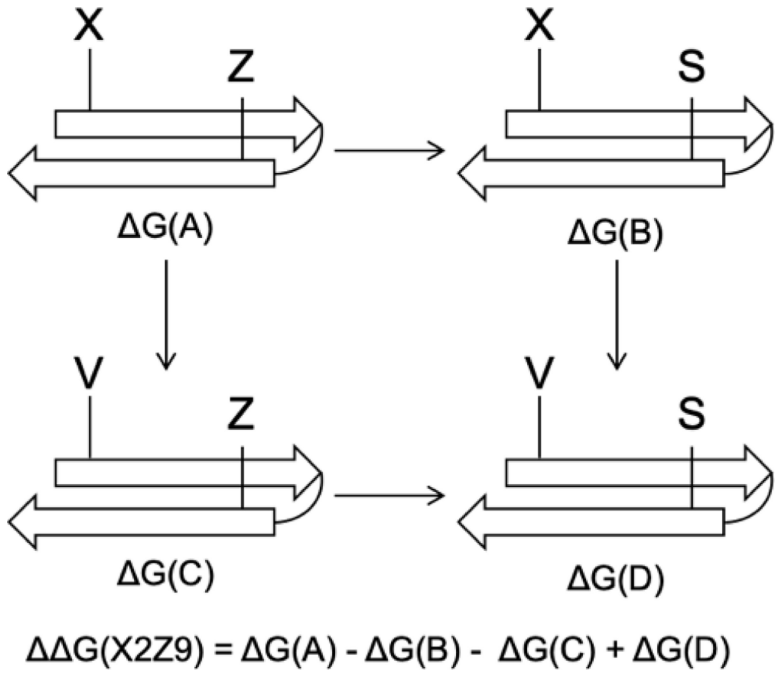

Figure 3.
Double mutant cycle used to measure the interaction energy between the X2 and Z9 residues. X2 and Z9 are replaced with Val and Ser respectively.

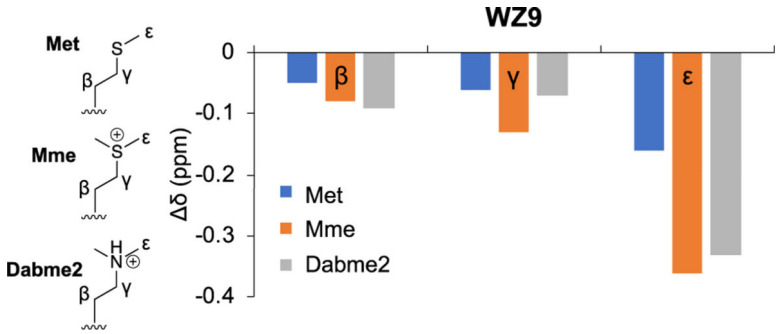

Figure 4.

Upfield shifting of WZ9 sidechain protons relative to random coil values. Met chemical shifts are colored in blue, Mme orange, and Dabme2 grey. Values calculated from data obtained at 293 K, 50 mM sodium acetate-d_3, pD 4.0 (uncorrected), referenced to DSS. Error in chemical shift is estimated to be ±0.01 ppm.

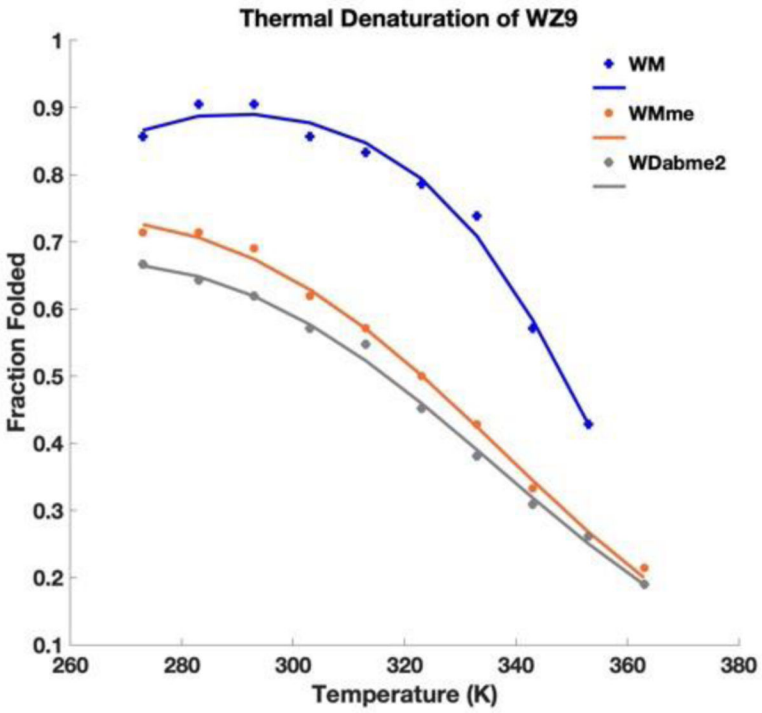

Figure 5.

Thermal denaturation plot of WZ9. The fraction folded is determined from reference compounds. The fitting of the curve was accomplished by using the following equation: fraction folded = (exp[X / RT])/1 + exp[X / RT]), where x= $\left[\Delta S_{298}^{\circ} + \Delta C_p^{\circ} ln\left\{\frac{T}{298}\right\}\right] - \Delta H_{298}^{\circ} + \Delta C_p^{\circ}\left[T - 298\right]$. Error is ±0.5 K in the temperature and 1–2% in the fraction folded. The estimated error in the fit is 15%.

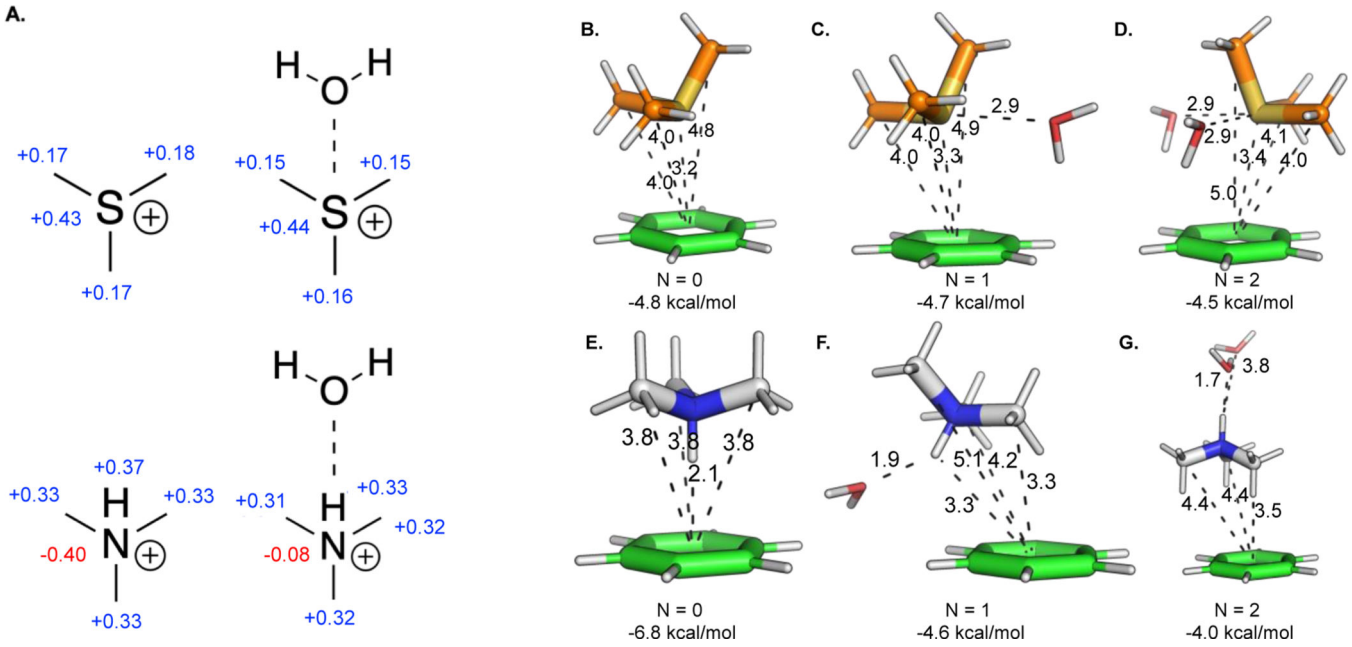

Figure 6.

(A) CM5 partial charge calculations for trimethylsulfonium, trimethylsulfonium interacting with water, trimethylammonium, and trimethylammonium hydrogen bonding with water. Optimized geometries of benzene with trimethylsulfonium (B-D) and trimethylammonium (E-G) with N = 0, 1, and 2 water molecules calculated at the M06–2X/6–311+G(d,p), CPCM (Water) level of theory. Interaction energy calculations were performed at the same level of theory.

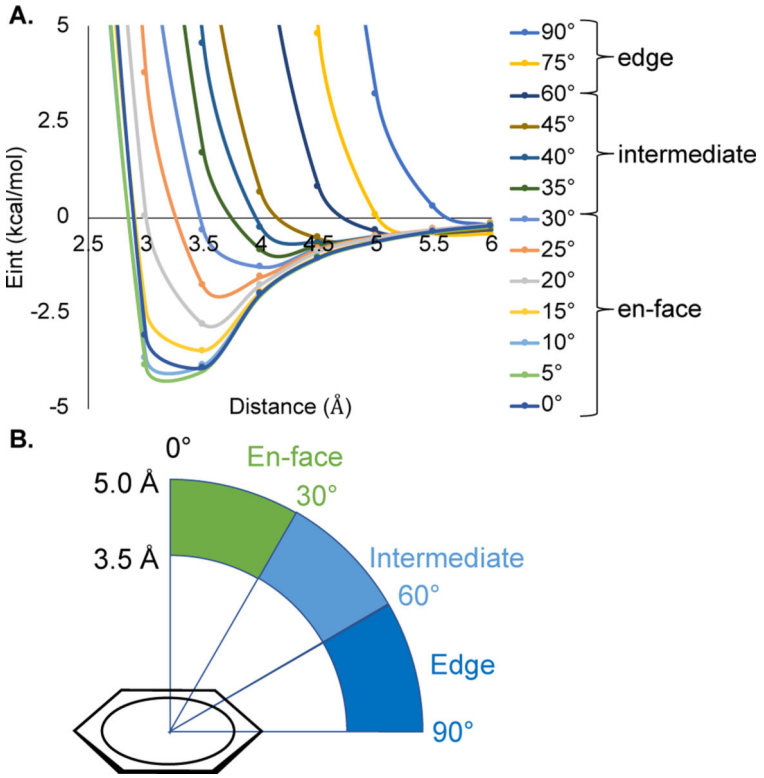

Figure 7.

(A) E_{int} of trimethylsulfonium-benzene as a function of distance. Calculations were computed at the M06–2X/6–311+G(d,p), CPCM(Water) level of theory. (B) Depiction of a 2D slice of angle and distance classifications for these analyses. Angles were measured relative to normal to the ring. Distances and angles were measured from the centroid of the ring to atoms discussed in the text.

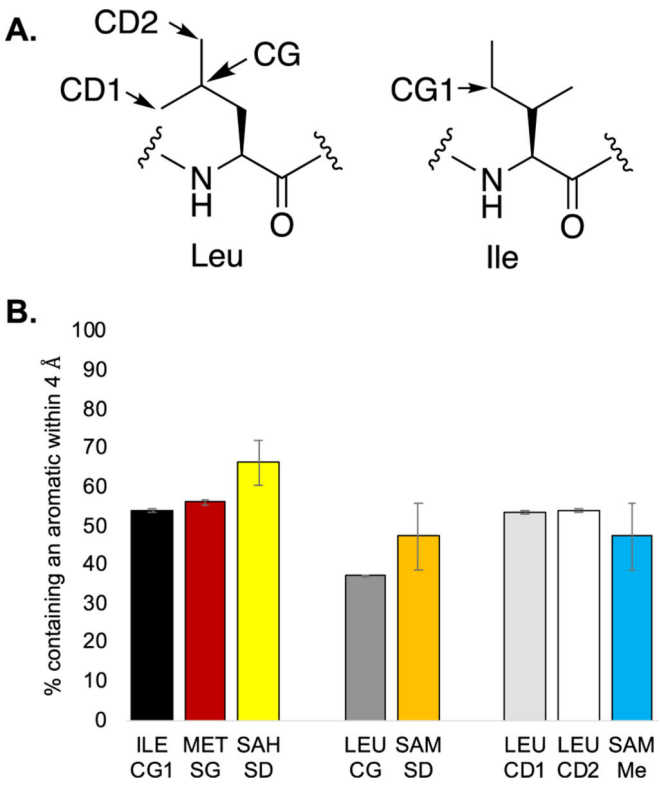

Figure 8.

(A) Structures of Leu and Ile with relevant positions labeled. (B) Percentage of atoms that form contacts < 4 Å to any aromatic sidechain atom, given a buried environment (24 ≤ # neighbors < 27) for individual atoms in Ile, Leu, Met sidechains and SAM and SAH cofactors. Neighbors are defined based on CB-CB distances (for amino acids) or C4'-CB distances (for cofactors) less than 10 Å. The aromatic contacts to S of SAH were compared to the electronically distinct but sterically similar CG1 of Ile and S of Met. Aromatic contacts to S of SAM were compared to CG of Leu. The aromatic contacts to Me of SAM were compared to electronically distinct but sterically similar CD1 and CD2 of Leu.

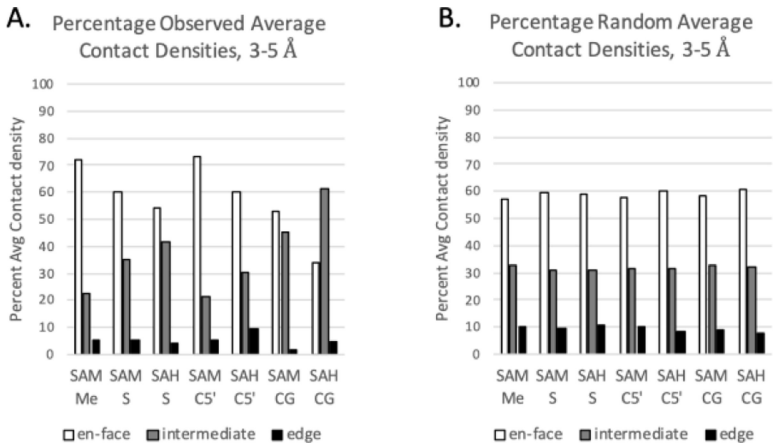

Figure 9.

Percent average contact densities of en-face, intermediate, and edge interactions to atoms in SAM and SAH contacts within 3–5 Å in a) observed- and b) random, collision-free structures. The preference for en-face over edge is visible in both datasets, but more pronounced in the observed data. For each position, the sum of en-face, intermediate, edge geometries totals 100%.

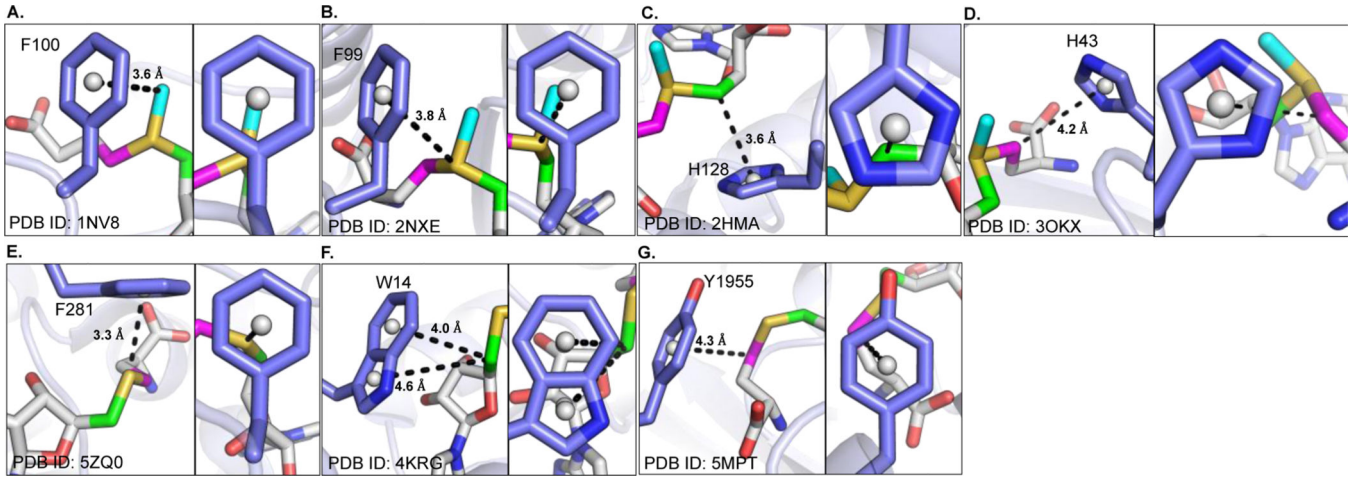

Figure 10.

Side- and normal-view of representative interactions of an aromatic residue to (A) Me (of SAM (cyan) – en-face, (B) S of SAM, (yellow) – intermediate (C) C5’ of SAM (green) – en-face, (D) CG of SAM (magenta) – intermediate, (E) S of SAH (yellow) – en-face, (F) C5’ of SAH – intermediate (green), and (G) CG of SAH (magenta) – intermediate.

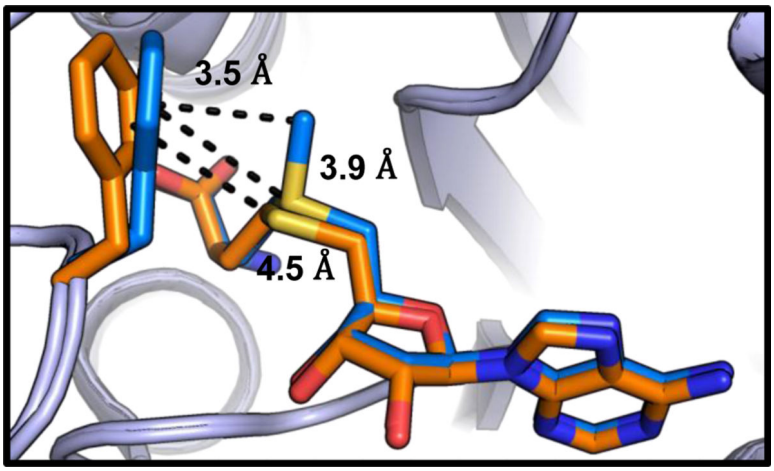

Figure 11.

Overlay of T. thermophilus ribosomal protein L11 methyltransferase (PrmA) bound to SAM (PDB ID: 2NXE, F99, SAM - cyan) and SAH (PDB ID: 3EGV, F99, SAH - green). Structures overlay with RMSD = 0.33 Å. F99 interacts with Me of SAM (3.5 Å) but reorients to move away (4.5Å) in the SAH bound structure.

Table 1.

Calculated polarizability values for Met, Mme, and Dabme2 sidechains.

Amino Acid	Met	Mme	Dabme2
Polarizability (10^{-30} m^3)	47.9	49.8	49.0

Polarizability of Met, Mme, and Dabme2 calculated at M06–2X/6–311+G(d,p) level of theory.

Table 2.

Fraction folded for β-hairpin peptides.

	% Folded (Gly)[a]	% Folded (Hα)[b]
WM	88	84
WMme	64	62
WDabme2	57	57
YM	76	67
YMme	36	50
YDabme2	38	48
FM	67	60
FMme	21	34
FDabme2	24	42

Values calculated from data obtained at 293 K, 50 mM sodium acetate-d3, pD 4.0 (uncorrected), referenced to sodium trimethylsilylpropane sulfonate (DSS).

[a] Error is 1% as determined from the error in chemical shift. For Mme and Dabme2, error is 2%

[b] Percent folded from Hα values is the average of the values from residues 3, 8, and 10.

[c] ΔG° calculated from fraction folded determined from Gly splitting.

Table 3.

Fraction folded for β-hairpin peptides.

	Diagonal Interaction	ΔΔG° (kcal/mol)[a]
WM	Trp-Met	−0.5
WMme	Trp-Mme	−1.4
WDabme2	Trp-Dabme2	−0.2
YM	Tyr-Met	−0.3
YMme	Tyr-Mme	−1.0
YDabme2	Tyr-Dabme2	−0.1
FM	Phe-Met	−0.3
FMme	Phe-Mme	−0.9
FDabme2	Phe-Dabme2	0.1

Values calculated from data obtained at 293 K, 50 mM sodium acetate-d3, pD 4.0 (uncorrected), referenced to DSS.

[a]Error is estimated at 0.1 kcal/mol for Met interactions, and 0.2 kcal/mol for Mme and Dabme2 due to the low degree of folding for some peptides in the double mutant cycle.

Table 4.

Thermodynamic parameters for folding for β-hairpin peptides.

	ΔH°' (kcal/mol)[a]	ΔS°' (cal/molK)[a]	ΔCp°' (cal/molK)[a]
WM	−2.2±0.3	−3.2±0.5	−260±40
WMme	−3.5±0.4	−11±2	−100±20
WDabme2	−3.1±0.5	−10±2	−100±20

Values calculated from data obtained from 273K to 363K, 50 mM sodium acetate-d_3, pD 4.0 (uncorrected), referenced to DSS.

[a]Error is estimated as 15% from error in the fit.